




Characterization of magnetic Fe₃O₄@SiO₂ nanoparticles with fluorescent properties for potential multipurpose imaging and theranostic applications

Nurdan Kurnaz Yetim^{1,*} , Fatma Kurşun Baysak¹, Mümin Mehmet Koç², and Dilek Nartop³

¹Department of Chemistry, Faculty of Arts and Sciences, Kırklareli University, Kırklareli, Turkey

²School of Medical Service, Kırklareli University, Kırklareli, Turkey

³Department of Polymer Engineering, Faculty of Technology, Düzce University, Düzce, Turkey

Received: 22 July 2020

Accepted: 27 August 2020

Published online:

8 September 2020

© Springer Science+Business Media, LLC, part of Springer Nature 2020

ABSTRACT

Fe₃O₄ magnetic nanoparticles (MNPs) were produced using hydrothermal synthesis and coated with tetraethyl orthosilicate (TEOS) where Fe₃O₄@SiO₂ MNPs with fluorescent properties were obtained. Structural characterization of the nanoparticles was performed using X-ray diffraction, scanning electron microscopy and transmission electron microscopy. Structural investigations confirmed that nanoparticles were in core@shell form. Chemical characterizations were performed using Fourier-transform infrared spectroscopy and energy-dispersive X-ray spectroscopy. Chemical investigations confirm that TEOS coating was successfully formed SiO₂ shells on Fe₃O₄ nanoparticles. Magnetic characterizations revealed that nanoparticles show superparamagnetic properties which make them a suitable candidate for magnetic hyperthermia and magnetic resonance imaging (MRI) applications. Increased thickness of SiO₂ shell in nanoparticle structure results in decreased magnetic saturation values. Fluorescence properties of the nanoparticles were confirmed using fluorescence spectroscopy. Increased SiO₂ shell thickness results in increased fluorescent intensity. It was confirmed that Fe₃O₄@SiO₂ nanoparticle has the potential to be used in medical applications such as MRI, fluorescence imaging and magnetic hyperthermia, and so on.

1 Introduction

Nanorange is a world that is full of surprises. Nanomaterials are building blocks of such a fascinating world and are under investigation of scientists

from different fields. Different properties of materials were revealed by scientists. Different parameters such as size, compound elements, structure, dimensions, and so on affect the properties and characteristics of the nanomaterials [1–4]. Metallic

Address correspondence to E-mail: nurdankurnazyetim@klu.edu.tr

nanoparticles find immense areas of application. They present outstanding electrical, magnetic, and optic properties that can be tuned with small modifications [5–10]. Such properties can be applied to different fields such as cancer therapy, targeted drug delivery, biomarking, catalysis reactions, supercapacitors fuel cells, etc. [11–16].

Iron oxide nanoparticles have great potential to be used in industrial and medical applications [14]. Iron oxide nanoparticles have magnetic properties [17, 18]. They can show superparamagnetic or ferromagnetic characteristics depending on their size and production method. Due to their electron affinity, they can be used in catalytic reaction as a catalyser [19, 20]. Previously Fe_3O_4 nanoparticles in different form and composition were produced and their catalysis properties were illustrated [21, 22]. Iron oxide is magnetic catalysis materials that can be extracted from water by using a magnet where no physical filtration was needed [20]. Several reports illustrate that iron oxide nanoparticles can be used more than one type of medical applications [14]. For example, they can be used in hyperthermia applications [23]. It was evidenced that they can kill cancer cells when they are applied to cancerous tissues with an external magnetic field [24, 25]. Moreover, nanocomposites containing iron oxide were used in the MRI applications [14]. Since iron oxide nanoparticles have certain magnetic properties, they can cause MRI weighting [18]. When they were applied to a certain tissue, they can change the contrast of the MRI image [14]. Therefore, they were often addressed as MRI contrast agents in the literature. Nanoparticles having both therapeutic and diagnostic properties were called as theranostic nanoparticles. Iron oxide-based nanoparticles are excellent theranostic nanoparticles that they can be used in both imaging and therapy applications, simultaneously [14]. However, they have certain drawbacks. For instance, iron oxide nanoparticles have high electron affinity which makes them unstable. They can interact with other materials around them. In addition, they are toxic to the cells, especially to the liver cells [14, 25].

To reduce their toxicity, they were often coated with organic molecules such as polyethylene glycol (PEG), polyvinyl acetate (PVA), poly amidoamine (PAMAM), and so on. [11, 14, 26–28]. Certain reports illustrate that physical properties of the nanoparticles can also be altered coating nanoparticles with organic molecules [29]. Coated organic molecules can then be

modified for targeted drug delivery applications [30–32]. However, the stability of such organic components was questioned; several reports claim that organic covers may decompose over time which can be a problem for in vivo applications. Alternatively, SiO_2 -based coatings were proposed in the literature [33–37]. SiO_2 has low toxicity and highly stable in the liquid environment [36, 38]. Si nanoparticles also used in medical and bioapplications [39–41]. They have fluorescent properties and used as biomarkers [39]. Moreover, various reports confirm that Si-based nanoparticles were used in fluorescence imaging (FI) applications as FI contrast agents [33, 35, 41].

In this report, magnetic Fe_3O_4 nanoparticles were produced using hydrothermal synthesis. Then, Fe_3O_4 magnetic nanoparticles (MNP) were covered with TEOS and $\text{Fe}_3\text{O}_4@ \text{SiO}_2$ MNPs in core@shell form were obtained. Morphologic properties of the nanoparticles were characterized using SEM and TEM. Crystal properties were assessed using XRD. The chemical composition of the MNPs was assessed using EDX and FTIR. Magnetic properties of the nanoparticles were assessed using vibrating sample magnetometry (VSM) and fluorescence properties were checked using fluorescence spectroscopy. Our investigations confirmed that $\text{Fe}_3\text{O}_4@ \text{SiO}_2$ nanoparticles were produced in core@shell form. They show superparamagnetic properties where increased SiO_2 coat thickness resulted in decreased magnetic properties. Increased SiO_2 thickness affects the fluorescence properties. It was concluded that fluorescence intensity increases with increasing SiO_2 shell thickness. It was evidenced that $\text{Fe}_3\text{O}_4@ \text{SiO}_2$ nanoparticles show magnetic characteristics with fluorescence properties. Such properties make $\text{Fe}_3\text{O}_4@ \text{SiO}_2$ nanoparticles a suitable candidate for MRI/FI multipurpose imaging applications. It was also illustrated that they have great potential to be used in theranostic applications.

2 Materials and methods

2.1 Spectral data measurements

Shimadzu IR Prestige 21 model spectrometer was used in the record of the Fourier transform infrared spectra in the scanning range between 450 and 4000 cm^{-1} . The RIGAKU miniflex600 X-ray diffraction device was used in the XRD assessment in the

range $10 < 2\theta < 90$. Scanning electron microscopy and energy-dispersive X-ray spectroscopy were used in the assessment of surface morphology. For SEM-EDX analysis, FEI Quanta FEG 250 model device was used. The JEOL 1220 JEM electron microscope was used in HR-TEM at an acceleration voltage of 200 kV. Magnetic measurements were performed at room temperature by a vibrating sample magnetometer, Cryogenic Limited PPMS with the maximum magnetic field of ± 1 T. Fluorescence measurements were performed using Photon Technology International Xeno Flash fluorescent spectrometer. Excitations in 250, 265, 300 and 310 nm wavelength were applied where emission wavelength between 0 and 700 nm was measured in a 0.450 slit. Measurements were performed in quartz cuvette in using the stirrer of fluorescence spectrophotometer.

2.2 Synthesis of Fe_3O_4 MNPs

1 g $\text{FeCl}_2 \cdot 4\text{H}_2\text{O}$ and 2.6 g $\text{FeCl}_3 \cdot 6\text{H}_2\text{O}$ were added to a bottom round balloon where 25 mL pure water was added and the solution was vent with Nitrogen gas. When they were totally solved, 28% NH_3 solution (10 mL) was dropwise added to the reaction pot. The solution was stirred in 60 °C for 2 h. Black precipitate was collected using a magnet and washed with pure water and ethyl alcohol (see Fig. 1). The result product was dried in vacuum conditions at 40 °C for 12 h [42].

2.3 The preparations of $\text{Fe}_3\text{O}_4@ \text{SiO}_2$ MNPs

MNPs were covered with TEOS. Following procedures were performed: 0.1 g Fe_3O_4 was added to 20 mL ethyl alcohol. They were sonicated for 30 min. Then, 0.5 mL TEOS and 0.5 mL 28% NH_3 solution were added to the solution. The solution was stirred at room temperature for 12 h at room temperature. MNPs were collected using a magnet. The collected precipitate was washed with pure water and ethyl alcohol. The result product was kept in a drying oven at 40 °C for 24 h under vacuum conditions (see Fig. 1). Same procedures were repeated for 1, 2 and 5 mL TEOS [43].

2.4 Fluorescence measurement

Fluorescent measurements were performed for TEOS-coated samples. For the fluorescence

measurement, 5 mg nanoparticle powder was dissolved in 10 mL dimethylformamide (DMF) solution. Initially, wavelength measurement was performed. Excitations in 250, 265, 300 and 310 nm were applied for the nanoparticle dispersion where emission wavelength was measured for 0–700 nm. The maximum fluorescent value was obtained for 300 nm excitation wavelength. Therefore, to assess the TEOS-related fluorescence, 300 nm excitation was used where emission was measured for 0–700 nm.

3 Result and discussion

3.1 Characterization of Fe_3O_4 and $\text{Fe}_3\text{O}_4@ \text{SiO}_2$ MNPs

3.1.1 XRD spectrum

XRD patterns of Fe_3O_4 MNPs are illustrated in Fig. 2. Apparent peaks were observed at 18.3°, 30.4°, 35.6°, 37.08°, 43.3°, 53.36°, 57.3°, 62.8°, 70.98°, 74.12°, 74.98° and 78.94° degrees which correspond to (1 1 1), (2 2 0), (3 1 1), (2 2 2), (4 0 0), (4 2 2), (5 1 1), (4 4 0), (6 2 0), (5 3 3), (6 2 2) and (4 4 4) face centred cubic crystal orientation, respectively [44]. Sharp peaks were observed XRD patterns of Fe_3O_4 which indicate that pure Fe_3O_4 MNPs were successfully produced using hydrothermal synthesis. No other contamination-related peak was seen. XRD patterns of TEOS-coated MNPs gives (2 2 0), (3 1 1), (4 0 0), (4 2 2), (5 1 1), (4 4 0), (6 2 0), (5 3 3), (6 2 2) and (4 4 4) peaks which were found to be similar to XRD peaks obtained for Fe_3O_4 MNPs. $\text{Fe}_3\text{O}_4@ \text{SiO}_2$ peaks were found to be broader than peaks of the Fe_3O_4 nanostructures. It was proposed that SiO_2 coat diminished the signals obtained from Fe_3O_4 nanoparticle. Observing similar XRD peaks for both Fe_3O_4 and $\text{Fe}_3\text{O}_4@ \text{SiO}_2$ nanostructures illustrates that Fe_3O_4 structure was protected in the core where SiO_2 cover does not alter the crystal structure of the magnetic Fe_3O_4 nanoparticles [27]. Since SiO_2 is in amorph structure, no SiO_2 -related peak was observed in the XRD pattern of $\text{Fe}_3\text{O}_4@ \text{SiO}_2$ nanostructures. A similar case was reported by Zarei et al. as well. Zarei et al. synthesized $\text{Fe}_3\text{O}_4@ \text{SiO}_2$ nanostructures and decorated them with carboxyl terminated PAMAM dendrimers [28]. In their report, peak positions in the XRD patterns of Fe_3O_4 and $\text{Fe}_3\text{O}_4@ \text{SiO}_2$ nanostructures were found to be identical. In addition, no SiO_2 -related peak was observed. It

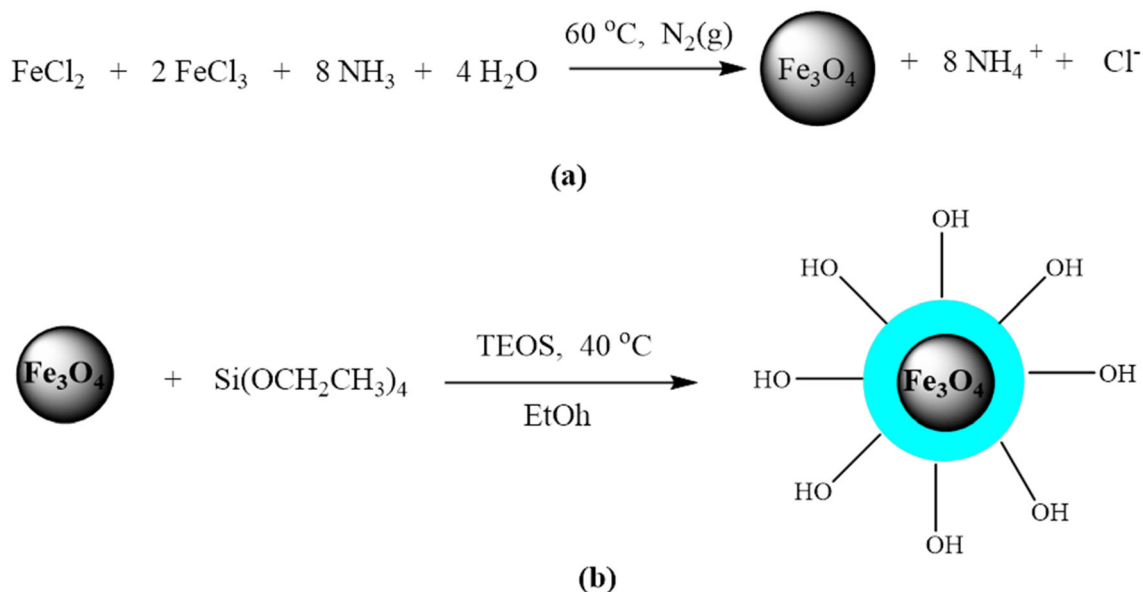


Fig. 1 Schematics of production of Fe₃O₄ magnetic nanoparticle core (a) and SiO₂ shell coating (b)

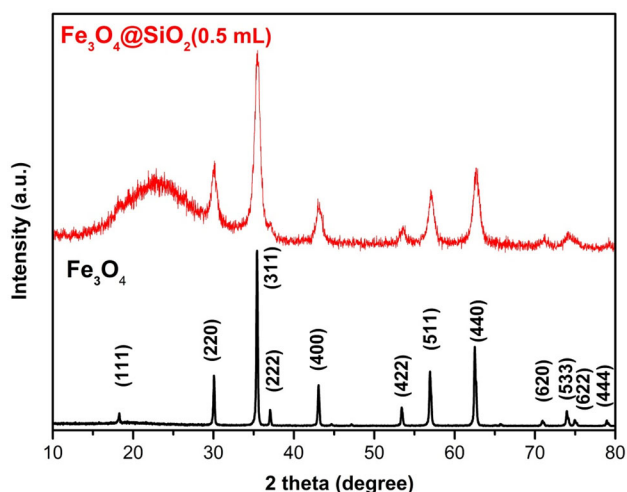


Fig. 2 XRD patterns of Fe₃O₄ and Fe₃O₄@SiO₂ MNPs

was concluded that SiO₂ coat does not change the crystal structure of the Fe₃O₄ magnetic nanostructures.

3.1.2 FTIR spectrum

The chemical structure of the MNPs was confirmed using FTIR spectroscopy. Figure 3 illustrates FTIR spectra of Fe₃O₄ and Fe₃O₄@SiO₂ MNPs. FTIR spectrum of Fe₃O₄ nanoparticles shows bands at 583 and 456 cm⁻¹ which were associated to internal tension peaks of metal that can be seen in the octahedral and tetrahedral region [45, 46].

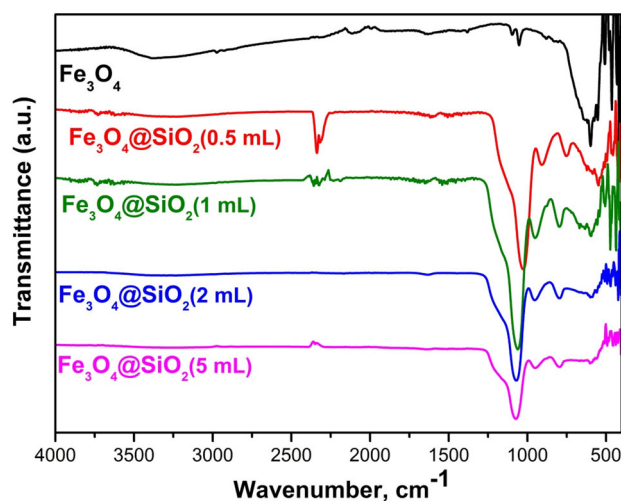


Fig. 3 FTIR spectra of pure Fe₃O₄ and TEOS-coated Fe₃O₄ MNPs

The band was observed at 562 cm⁻¹ for the SiO₂-coated Fe₃O₄ nanoparticles associated with Fe–O stretching vibration. The band is a characteristic band which illustrates Fe–O tension in octahedral orientation. For the FTIR spectrum of a pure Fe₃O₄ nanostructure, the band was observed at 558 cm⁻¹. A slight difference obtained in the FTIR spectrum of Fe₃O₄@SiO₂ was attributed to the TEOS coat. Peaks observed at 1053, 948 and 795 cm⁻¹ also confirm the existence of TEOS coating which indicates Si–O–Si stretching vibration peaks [43]. Wideband observed

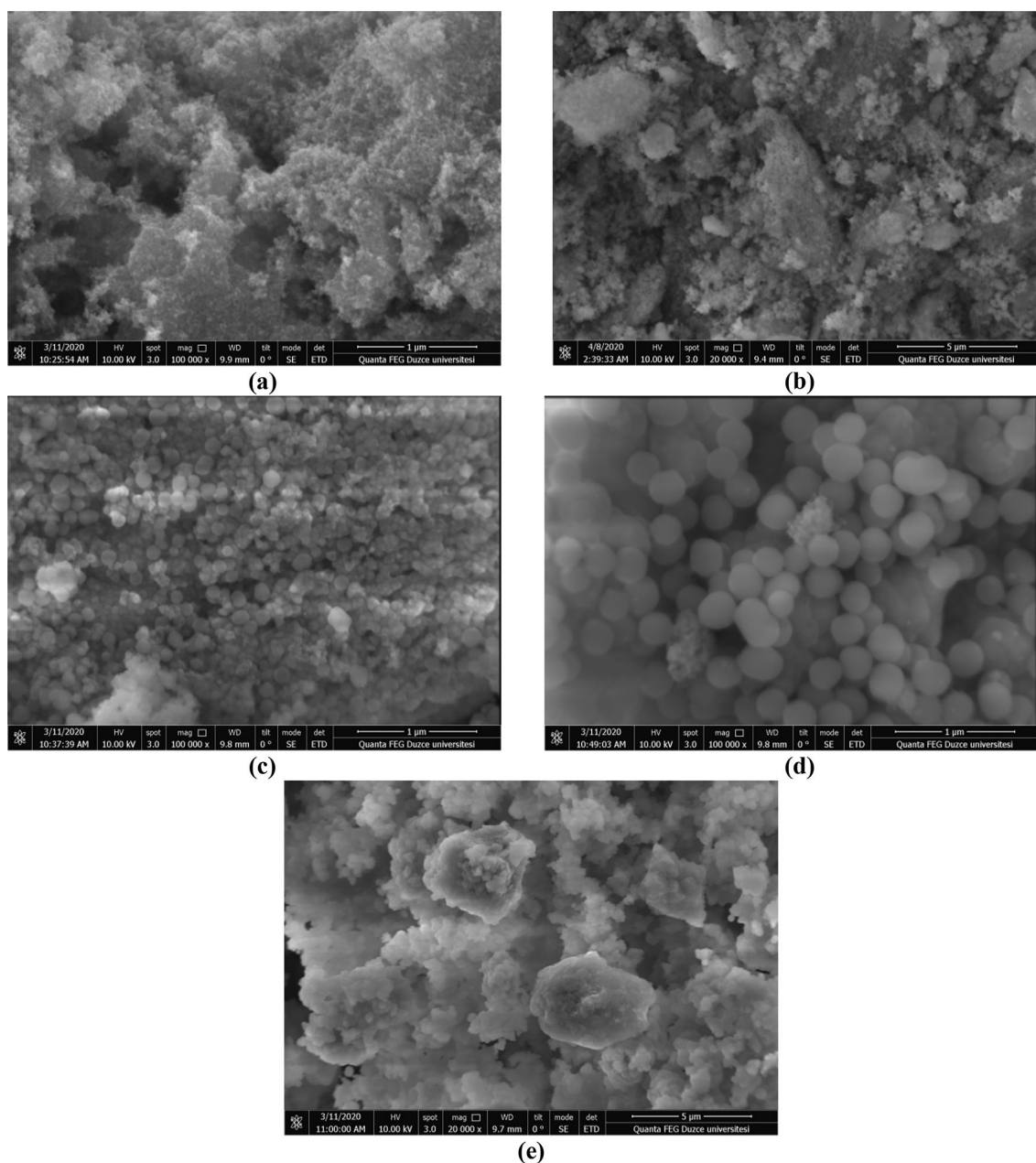


Fig. 4 SEM images obtained from pure Fe₃O₄ (a) and 0.5 mL TEOS (b), 1 mL TEOS (c), 2 mL TEOS (d), 5 mL TEOS (e)-coated Fe₃O₄@SiO₂ MNPs

at 3000–3500 cm⁻¹ illustrates silanol (Si–OH) and H–OH-related stretching vibrations [43].

3.1.3 SEM-TEM images and EDX spectrum

Microscopic investigations of Fe₃O₄, Fe₃O₄@SiO₂ and Fe₃O₄@SiO₂/NH₂ MNPs were performed using scanning electron microscopy and transmission electron microscopy. EDX analysis was also performed to confirm the chemical structure of the

nanoparticles. Figure 4 illustrates the Fe₃O₄ and SiO₂-coated Fe₃O₄ nanoparticles. SEM images revealed that Fe₃O₄ MNPs were formed in cubic structures. It was also seen in the SEM images that Fe₃O₄ nanoparticles agglomerated due to their magnetic characteristics. SEM images of 0.5 mL, 1 mL, 2 mL and 5 mL TEOS-coated Fe₃O₄ nanoparticles are also presented in Fig. 4b–e, respectively. Visual inspections revealed that TEOS coating makes the shapes of Fe₃O₄ nanoparticles spherical. However, increased

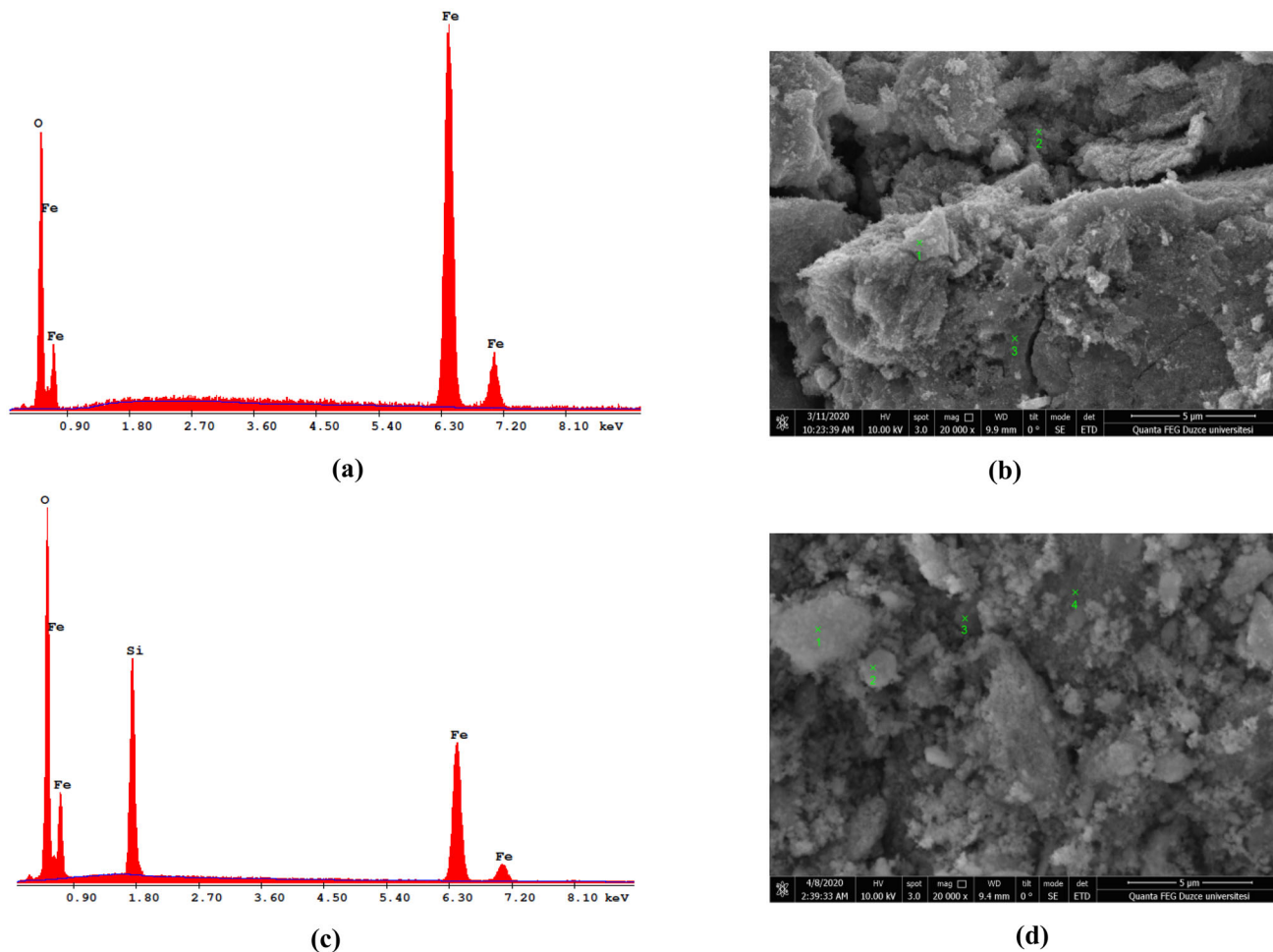


Fig. 5 EDX spectra (a) and SEM image (b) of Fe₃O₄ and; EDX spectra (c) and SEM image (d) of 0.5 mL TEOS-coated Fe₃O₄@SiO₂ (b) nanoparticles. Points, where EDX spectra were obtained, were marked with green numbers in the SEM images

Table 1 EDX results of MNPs

Nanoparticle type	C (%)	N (%)	O (%)	Si (%)	Fe (%)
Fe ₃ O ₄	N.D	N.D	16.36	–	83.64
Fe ₃ O ₄ @SiO ₂ (0.5 mL)	N.D	N.D	35.29	18.00	46.71
Fe ₃ O ₄ @SiO ₂ (1 mL)	N.D	N.D	37.00	28.22	34.77
Fe ₃ O ₄ @SiO ₂ (2 mL)	N.D	N.D	46.99	31.03	21.98
Fe ₃ O ₄ @SiO ₂ (5 mL)	N.D	N.D	49.70	38.79	11.51

N.D not detected

TEOS amount results in deformation in the spherical shape. EDX analysis of the MNPs is presented in Fig. 5. It can be seen from EDX analysis that Fe₃O₄ nanoparticles give apparent Fe and O-related peaks where no other contamination-related peak can be seen. EDX results of TEOS-coated Fe₃O₄ nanoparticles are presented in Fig. 5b. Clear Si, Fe and O peaks were detected. Chemical concentrations of Fe₃O₄ and Fe₃O₄@SiO₂ MNPs were assessed using EDX and

results are presented in Table 1. It was evidenced that increased TEOS amount increased the concentration of Si in the structure of Fe₃O₄@SiO₂. Such a case is related to the thickness of SiO₂ cover in the structure of Fe₃O₄@SiO₂ nanoparticles.

TEM images of Fe₃O₄ and Fe₃O₄@SiO₂ MNPs are presented in Fig. 6. The figure clearly illustrates the core@shell structure of the Fe₃O₄@SiO₂ nanoparticles. TEM images confirm that Fe₃O₄ nanoparticles were

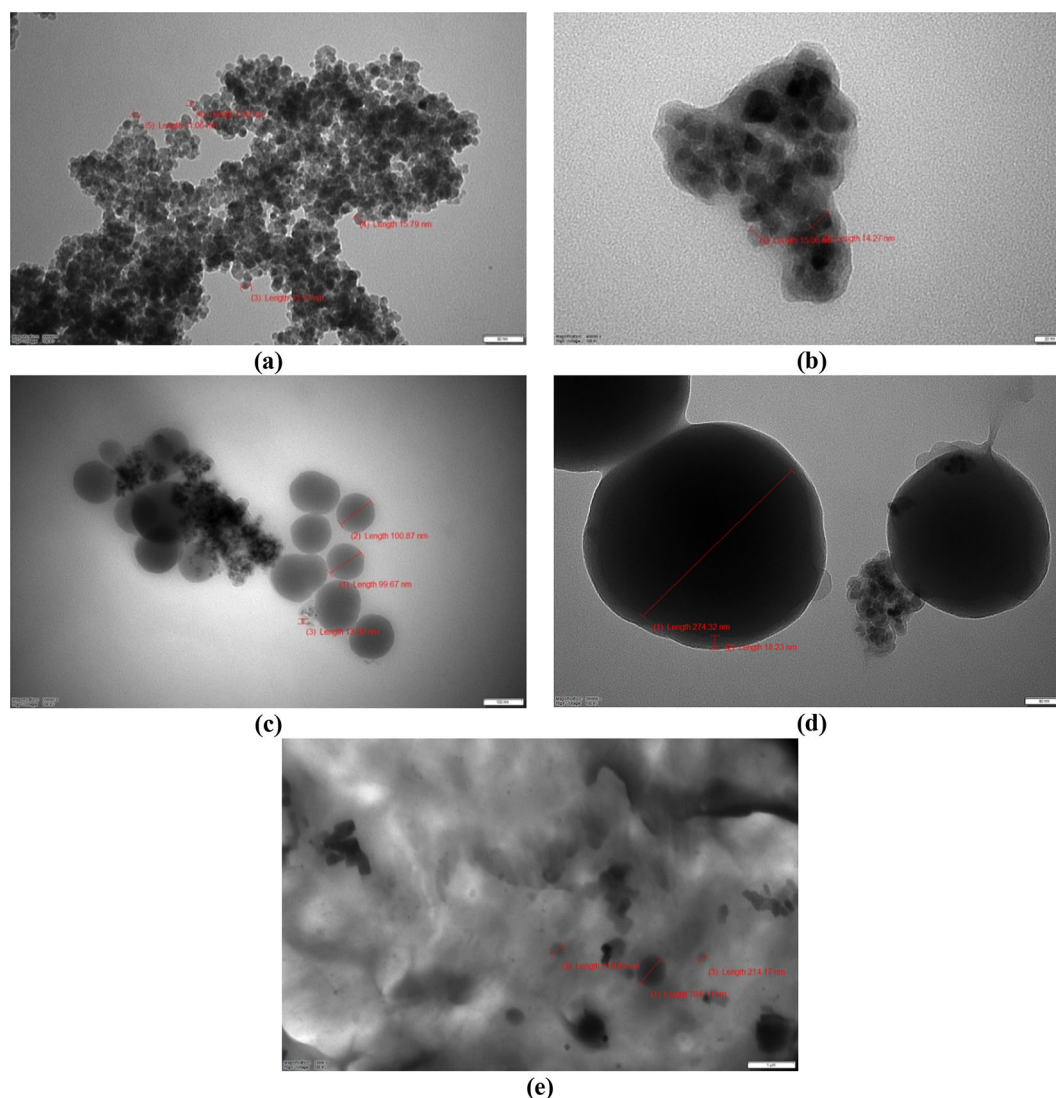


Fig. 6 TEM images of pure Fe_3O_4 (a) and 0.5 mL TEOS (b), 1 mL TEOS (c), 2 mL TEOS (d), 5 mL TEOS (e)-coated $\text{Fe}_3\text{O}_4@SiO_2$ MNPs

perfectly coated with SiO_2 where the core@shell $\text{Fe}_3\text{O}_4@SiO_2$ structure was successfully obtained. TEM images of Fe_3O_4 revealed that the size of a single Fe_3O_4 nanoparticle is about 11.7 nm that they were found to be in the agglomerated form (see Fig. 6a). The size of $\text{Fe}_3\text{O}_4@SiO_2$ nanoparticles was found to be 15.06 nm for 0.5 mL TEOS (Fig. 6b), 100 nm for 1 mL TEOS (Fig. 6c), 270 nm for 2 mL TEOS (Fig. 6d) and 412.3 nm for 5 mL TEOS (Fig. 6e), respectively. The increased size was obtained with increased TEOS amount which was found to be coherent with our EDX results.

3.1.4 Magnetic measurement of Fe_3O_4 and $\text{Fe}_3\text{O}_4@SiO_2$ MNPs

Magnetic hysteresis curves of Fe_3O_4 and $\text{Fe}_3\text{O}_4@SiO_2$ are presented in Fig. 7. It was seen in the magnetic hysteresis curves that Fe_3O_4 and $\text{Fe}_3\text{O}_4@SiO_2$ nanoparticles have superparamagnetic characteristics. The magnetic saturation value of Fe_3O_4 MNPs was found to be 63.7 emu/g. The magnetic saturation values of $\text{Fe}_3\text{O}_4@SiO_2$ nanoparticles were found to be 48.7 emu/g for 0.5 mL TEOS, 23.9 for 1 mL TEOS, 17.3 emu/g for 2 mL TEOS and 8.99 emu/g for 5 mL TEOS, respectively. It was illustrated that increased thickness of SiO_2 coat in the $\text{Fe}_3\text{O}_4@SiO_2$ structure reduces the magnetic saturation values of the

nanoparticles. It was suspected that SiO₂ coat thickness shadows the measured magnetization. Previously different magnetic saturation values were reported in the literature for Fe₃O₄-based

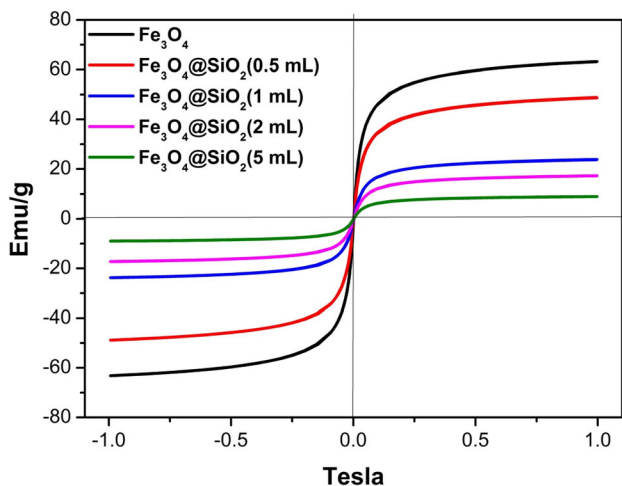


Fig. 7 Magnetic hysteresis curves of Fe₃O₄ and Fe₃O₄@SiO₂ MNPs

Table 2 Magnetic saturation values reported in the literature for the Fe₃O₄-based nanoparticles and nanocomposites

Nanoparticle type	Magnetic saturation value (emu/g)	References
Fe ₃ O ₄	18.4–90.4	[47, 48]
Fe ₃ O ₄ /gelatine/metoprolol	3.5	[32]
Fe ₃ O ₄ /gelatine/aspirin	8	[32]
Fe ₃ O ₄ -PbS	8.2	[22]
Silica coated Fe ₃ O ₄	36.2	[43]
PDA coated Fe ₃ O ₄	28.5	[43]
Silver coated Fe ₃ O ₄	22.5	[43]
Fe ₃ O ₄ @SiO ₂ (our nanoparticles)	8.99–48.7	–
Bi ₂ S ₃ @Fe ₃ O ₄	0.65–12.6	[47, 48]

nanocomposites and some of them are reported in Table 2. For example, magnetic saturation of Fe₃O₄-PbS nanostructures was found to be 8.2 emu/g [22]; magnetic saturation values of Bi₂S₃@Fe₃O₄ were found to be between 2.24 and 28.6 emu/g [47]; magnetic saturation values of Fe₃O₄/gelatine/metoprolol and Fe₃O₄/gelatine/aspirin were found to be 3.5 emu/g and 8 emu/g, respectively [32]. Magnetic saturation values of Fe₃O₄ and Fe₃O₄@SiO₂ were previously reported between 62.2 and 22.21 emu/g [43]. It was concluded that magnetic saturation values of our nanoparticles were in good agreements values reported in the literature.

3.1.5 Photofluorescence spectra

It was previously mentioned in the introduction that Si-based nanoparticles exhibit fluorescence properties. Therefore, fluorescence properties of the nanoparticles were assessed using fluorescence spectroscopy and are presented in Fig. 8. To assess

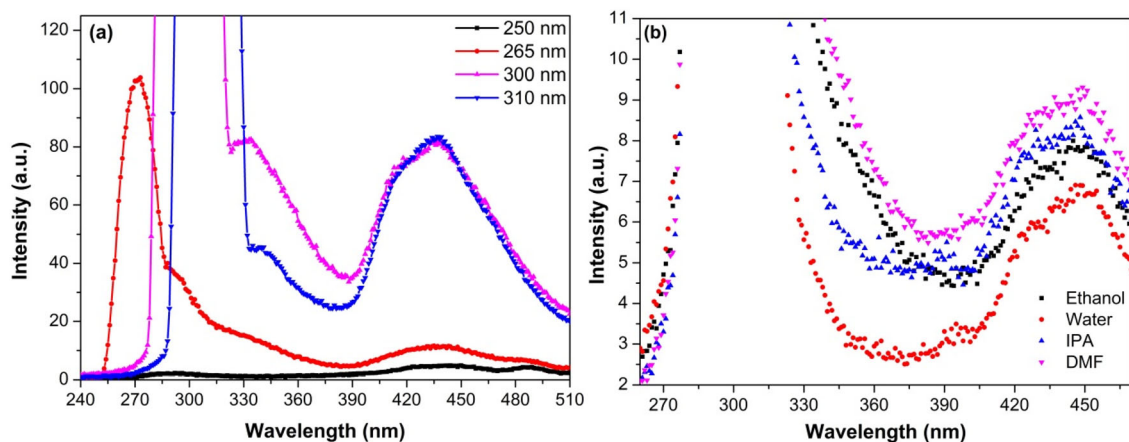


Fig. 8 Fluorescence excitation spectra of oxidized Fe₃O₄@SiO₂ (5 mL) MNp in DMF (a) and fluorescence spectra of Fe₃O₄@SiO₂ (5 mL) MNp in different solvents (b) (λ_{exc} = 300 nm)

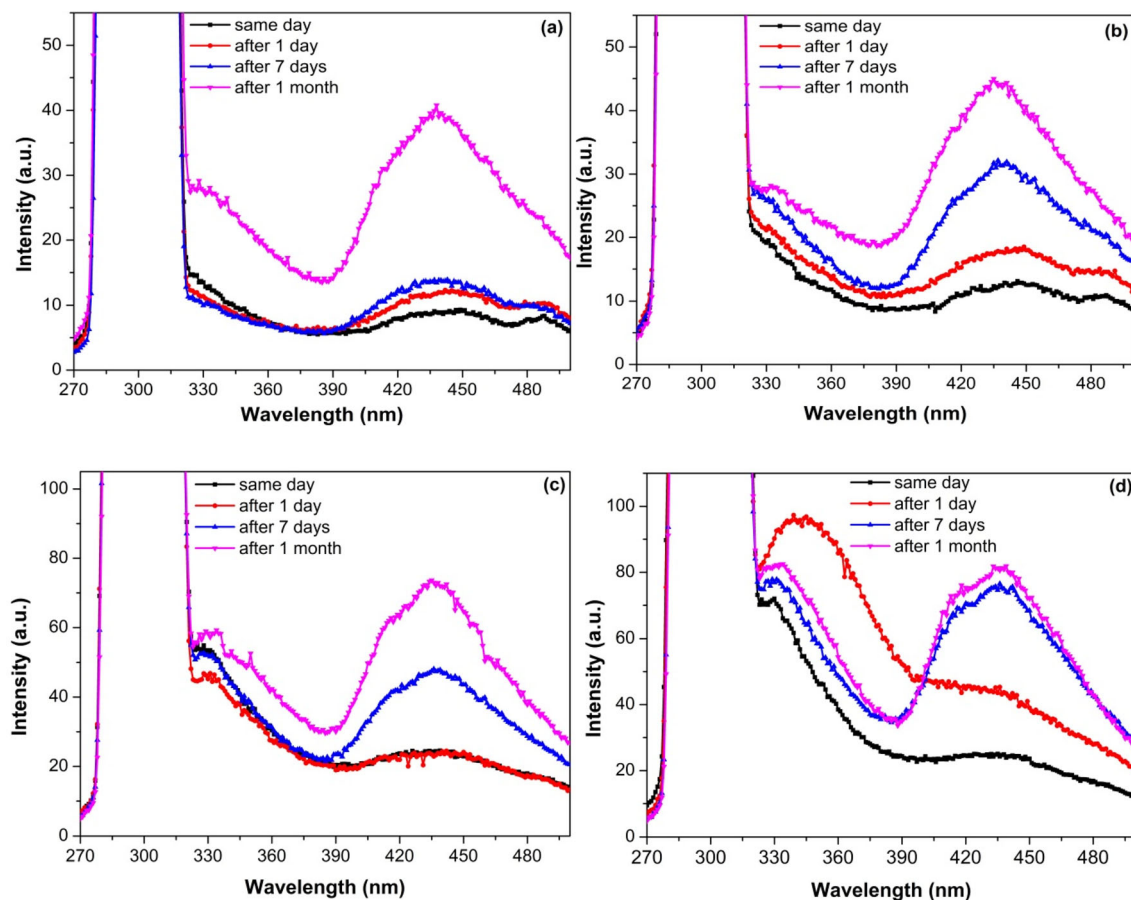


Fig. 9 Time-related fluorescence properties of **a** $\text{Fe}_3\text{O}_4@\text{SiO}_2$ (0.5 mL TEOS coat), **b** $\text{Fe}_3\text{O}_4@\text{SiO}_2$ (1 mL TEOS coat), **c** $\text{Fe}_3\text{O}_4@\text{SiO}_2$ (2 mL TEOS coat), **d** $\text{Fe}_3\text{O}_4@\text{SiO}_2$ (5 mL TEOS coat) nanoparticles dissolved in DMF ($\lambda_{\text{exc}} = 300 \text{ nm}$)

the fluorescence properties, different excitation wavelengths (250 nm, 265 nm, 300 nm, 310 nm) were performed for $\text{Fe}_3\text{O}_4@\text{SiO}_2$ (5 mL) in DMF. Nanoparticles were produced in nanopowder form. Highest fluorescence was obtained in 300 nm excitation wavelength where the apparent peak was observed at around 450 nm. To investigate the solvent effect on fluorescence properties, nanoparticles were dissolved in different solvents such as water, ethanol, isopropanol (IPA) and DMF. It was illustrated that nanoparticles dissolved in DMF give the highest intensity where nanoparticles in water give the lowest peak intensity. Fluorescent peaks were obtained at around 450 nm for all solvents that no solvent-related shift was obtained. Such a result indicates that nanoparticles were highly stable in different solutions and do not interact with solutions in a short period.

To check the stability of the nanoparticles, time-related fluorescence properties of the nanoparticles

were assessed. 5 mL nanoparticles with different TEOS coating was dissolved in DMF and fluorescence spectra of nanoparticles were obtained in different dates (on the same day, after 1 day, after 7 day and after 1 month). In Fig. 9, time-related fluorescence behaviours of $\text{Fe}_3\text{O}_4@\text{SiO}_2$ (0.5 mL TEOS coat), $\text{Fe}_3\text{O}_4@\text{SiO}_2$ (1 mL TEOS coat), $\text{Fe}_3\text{O}_4@\text{SiO}_2$ (2 mL TEOS coat) and $\text{Fe}_3\text{O}_4@\text{SiO}_2$ (5 mL TEOS coat) nanoparticles can be seen. It was seen in the figure that increased TEOS ingredient increases the fluorescence intensity. Apparent intensity difference can be seen for different TEOS concentrations. Moreover, time makes a positive effect on nanoparticle fluorescence intensity. The increased amount of time that nanoparticles spent in DMF results in increased intensity. Nanoparticles staying in DMF for 1 month give highest peak intensity while fluorescence peak intensity of the nanoparticles obtained in the same day as found to be lowest. A similar case was also reported by Brewer et al. where researchers

produce Si nanoparticles in liquid [38]. The luminescence intensity peak of their nanoparticles was also increased with time they spend in their liquid. It was found out that nanoparticles were highly stable and do not lose their fluorescent properties over time.

4 Conclusion

Fe₃O₄ nanoparticles were vastly used in medical and technological applications. In this work, Fe₃O₄ nanoparticles were produced and coated with TEOS where nanoparticles in Fe₃O₄@SiO₂ form was obtained. The structural and chemical characterizations of the nanoparticles were performed. Microscopic characterizations confirm the Fe₃O₄@SiO₂ core@shell structure. Magnetic characterization revealed that nanoparticles were in superparamagnetic form which makes them a suitable candidate for magnetic hyperthermia and MRI contrast agent applications. Increased SiO₂ shell thickness results in decreased magnetic saturation value. Fluorescent properties of the Fe₃O₄@SiO₂ nanoparticles were performed and it was revealed that nanoparticles have fluorescent characteristics. Different fluorescence intensities were achieved for different solutions. Increased thickness of SiO₂ nanoparticles results in increased fluorescence intensity. The longer Fe₃O₄@SiO₂ nanoparticles stay in DMF, the higher fluorescence intensity was achieved. It was concluded that our nanoparticles were stable in different solvents and preserve their fluorescent properties. It was concluded that our nanoparticles are a suitable candidate for multimodal imaging applications.

Acknowledgements

This work was supported by Duzce University Scientific Research Project Commission with Project Number 2019.07.06.981.

References

1. L. Babes, B. Denizot, G. Tanguy, J.J. Le Jeune, P. Jallet, J. Colloid Interface Sci. **212**, 474 (1999)
2. M. Daniel, D. Astruc, Chem. Rev. **1**, 293 (2004)
3. X. Xu, C. Xu, J. Dai, J. Hu, F. Li, S. Zhang, J. Phys. Chem. C **116**, 8813 (2012)
4. T.-J. Park, G.C. Papaefthymiou, A.J. Viescas, A.R. Moodenbaugh, S.S. Wong, Nano Lett. **7**, 766 (2007)
5. M. Fraune, U. Rüdiger, G. Güntherodt, S. Cardoso, P. Freitas, Appl. Phys. Lett. **77**, 3815 (2000)
6. S. Wang, W. Lu, O. Tovmachenko, U. Rai, H. Yu, Chem. Phys. Lett. **1**, 145 (2008)
7. A. Więckowski, E.R.E. Savinova, C.G. Vayenas, *Catalysis and Electrocatalysis at Nanoparticle Surfaces*, 1st edn. (Marcel Dekker, New York, 2003)
8. S.A. Kulkarni, P.S. Sawadh, P.K. Palei, K.K. Kokate, Ceram. Int. **40**, 1945 (2014)
9. M. Mahdi, A. Djabri, M.M. Koc, R. Boukhalfa, M. Erkovan, Y. Chumakov, F. Chemam, Mater. Sci. Pol. **37**, 182 (2019)
10. T. Rezkallah, I. Djabri, M.M. Koç, M. Erkovan, Y. Chumakov, F. Chemam, Chin. J. Phys. **55**, 1432 (2017)
11. L.E. Cole, T.L. McGinnity, L.E. Irimata, T. Vargo-Gogola, R.K. Roeder, Acta Biomater. **82**, 122 (2018)
12. E. Roduner, Chem. Soc. Rev. **35**, 583 (2006)
13. D. Yan, X. Liu, G. Deng, H. Yuan, Q. Wang, L. Zhang, J. Lu, J. Colloid Interface Sci. **530**, 547 (2018)
14. N. Aslan, B. Ceylan, M.M. Koç, F. Findik, J. Mol. Struct. **1219**, 128599 (2020)
15. N. Kurnaz Yetim, N. Aslan, A. Sarioğlu, N. Sarı, M.M. Koç, J. Mater. Sci. Mater. Electron. **31**, 12238 (2020)
16. N. Aslan, M.M. Koç, A. Dere, B. Arif, M. Erkovan, A.G. Al-Sehemi, A.A. Al-Ghamdi, F. Yakuphanoglu, J. Mol. Struct. **1155**, 813 (2018)
17. S. Aktas, S.C. Thornton, C. Binns, P. Denby, J. Nanoparticle Res. **18**, 365 (2016)
18. S. Aktas, S.C. Thornton, C. Binns, L. Lari, A. Pratt, R. Kröger, M.A. Horsfield, S. Aktas, S.C. Thornton, C. Binns, L. Lari, A. Pratt, R. Kröger, M.A. Horsfield, Mater. Res. Express **2**, 105356 (2015)
19. Y.C. Chang, D.H. Chen, J. Hazard. Mater. **165**, 664 (2009)
20. N. Kurnaz Yetim, N. Aslan, M.M. Koç, J. Environ. Chem. Eng. **8**, 104258 (2020)
21. K. Hedayati, M. Kord, M. Goodarzi, D. Ghanbari, S. Gharigh, Mater. Sci. Mater. Electron. **28**, 1577 (2017)
22. K. Hedayati, M. Goodarzi, M. Kord, Main Gr. Met. Chem. **39**, 183 (2016)
23. C. Binns, P. Prieto, S. Baker, P. Howes, R. Dondi, G. Burley, L. Lari, R. Kröger, A. Pratt, S. Aktas, J.K. Mellon, J. Nanoparticle Res. **14**, 1136 (2012)
24. Y. Liu, Z. Yang, X. Huang, G. Yu, S. Wang, Z. Zhou, Z. Shen, W. Fan, Y. Liu, M. Davison, H. Kalish, G. Niu, Z. Nie, X. Chen, ACS Nano **12**, 8129 (2018)
25. K.C. Barick, S. Singh, D. Bahadur, M.A. Lawande, D.P. Patkar, P.A. Hassan, J. Colloid Interface Sci. **418**, 120 (2014)
26. J. Suh, K. Choy, S. Lai, J. Suk, B. Tang, Int. J. Nanomed. **2**, 735 (2007)

27. G.H. Mirzabe, A.R. Keshtkar, *J. Ind. Eng. Chem.* **26**, 277 (2015)
28. A. Zarei, S. Saedi, F. Seidi, *J. Inorg. Organomet. Polym. Mater.* **28**, 2835 (2018)
29. K. Hedayati, M. Goodarzi, D. Ghanbari, *J. Nanostruct.* **7**, 32 (2017)
30. J.R. Ashton, E.B. Gottlin, E.F. Patz, J.L. West, C.T. Badea, *PLoS ONE* **13**, e0206950 (2018)
31. W. Eck, A.I. Nicholson, H. Zentgraf, W. Semmler, S. Bartling, *Nano Lett.* **10**, 2318 (2010)
32. F. Kavousi, M. Goodarzi, D. Ghanbari, K. Hedayati, *J. Mol. Struct.* **1183**, 324 (2019)
33. Z. Zhou, C. Zhang, Q. Qian, J. Ma, P. Huang, X. Zhang, L. Pan, G. Gao, H. Fu, S. Fu, H. Song, X. Zhi, J. Ni, D. Cui, *J. Nanobiotechnol* **11**, 17 (2013)
34. J.-H. Park, L. Gu, G. von Maltzahn, E. Ruoslahti, S.N. Bhatia, M.J. Sailor, *Nat. Mater.* **8**, 331 (2009)
35. S.-P. Kwon, S. Jeon, S.-H. Lee, H.Y. Yoon, J.H. Ryu, D. Choi, J.-Y. Kim, J. Kim, J.H. Park, D.-E. Kim, I.C. Kwon, K. Kim, C.-H. Ahn, *Biomaterials* **150**, 125 (2018)
36. F.-G. Wu, X. Zhang, S. Kai, M. Zhang, H.-Y. Wang, J.N. Myers, Y. Weng, P. Liu, N. Gu, Z. Chen, *Adv. Mater. Interfaces* **2**, 1500360 (2015)
37. Y. Park, A. Kasuya, A. Dmytruk, N.N. Yasuto, *J. Nanosci. Nanotechnol.* **8**, 2690 (2007)
38. A. Brewer, K. von Haefen, *Appl. Phys. Lett.* **94**, 261102 (2009)
39. S. Santra, P. Zhang, K. Wang, R. Tapeç, W. Tan, *Anal. Chem.* **73**, 4988 (2001)
40. S. Xue, Y. Wang, M. Wang, L. Zhang, X. Du, *Int. J. Nanomed* **9**, 2527 (2014)
41. M.M. van Schooneveld, D.P. Cormode, R. Koole, J.T. van Wijngaarden, C. Calcagno, T. Skajaa, J. Hilhorst, DC't Hart, Z.A. Fayad, W.J.M. Mulder, A. Meijerink, *Contrast Media Mol. Imaging* **5**, 231 (2010)
42. S. Kulkarni, P. Sawadh, P. Palei, *J. Korean Chem* **58**, 100 (2014)
43. H. Tumturk, F. Sahin, E. Turan, *Analyst* **139**, 1093 (2014)
44. R.Y. Hong, S.Z. Zhang, G.Q. Di, H.Z. Li, Y. Zheng, J. Ding, D.G. Wei, *Mater. Res. Bull.* **43**, 2457 (2008)
45. W. Lei, Y. Liu, X. Si, J. Xu, W. Du, J. Yang, T. Zhou, J. Lin, *Phys. Lett. Sect. A Gen. At. Solid State Phys.* **381**, 314 (2017)
46. F. Qu, Y. Wang, J. Liu, S. Wen, Y. Chen, S. Ruan, *Mater. Lett.* **132**, 167 (2014)
47. R. Karaçam, N.K. Yetim, M.M. Koç, *J. Supercond. Nov. Magn.* **33**, 2715 (2020)
48. H. Zhu, R. Jiang, J. Li, Y. Fu, S. Jiang, J. Yao, *Sep. Purif. Technol.* **179**, 184 (2017)

Publisher's Note Springer Nature remains neutral with regard to jurisdictional claims in published maps and institutional affiliations.